Measurements of ion cyclotron range of frequencies mode converted wave intensity with phase contrast imaging in Alcator C-Mod and comparison with full-wave simulations

Measurements of ICRF Mode Converted Wave Intensity with Phase Contrast Imaging in Alcator C-Mod and Comparison with Full-Wave Simulations

N. Tsujii,[1, a)] M. Porkolab,[1] P. T. Bonoli,[1] Y. Lin,[1] J. C. Wright,[1] S. J. Wukitch,[1]
E. F. Jaeger,[2] D. L. Green,[3] and R. W. Harvey[4]

[1)]*MIT Plasma Science and Fusion Center, Cambridge, Massachusetts 02139,
USA*

[2)]*XCEL Engineering, Inc., Oak Ridge, Tennessee 37830,
USA*

[3)]*Oak Ridge National Laboratory, Oak Ridge, Tennessee 37831,
USA*

[4)]*CompX, Del Mar, California 92014, USA*

(Dated: 24 July 2012)

Radio frequency waves in the ion cyclotron range of frequencies (ICRF) are widely used to heat tokamak plasmas. In ICRF heating schemes involving multiple ion species, the launched fast waves convert to ion cyclotron waves or ion Bernstein waves at the two-ion hybrid resonances. Mode converted waves are of interest as actuators to optimise plasma performance through current drive and flow drive. In order to describe these processes accurately in a realistic tokamak geometry, numerical simulations are essential, and it is important that these codes be validated against experiment. In this study, the mode converted waves were measured using a phase contrast imaging technique in D-H and D-^{3}He plasmas. The measured mode converted wave intensity in the D-^{3}He mode conversion regime was found to be a factor of $\sim$50 weaker than the full-wave predictions. The discrepancy was reduced in the hydrogen minority heating regime, where mode conversion is weaker.

[a)]ntsujii@psfc.mit.edu

I. INTRODUCTION

Radio frequency (rf) waves in the ion cyclotron range of frequencies (ICRF) are widely used to heat fusion plasmas. Unlike electron cyclotron waves or lower hybrid waves, ICRF fast waves do not have any accessibility issues at high density, which becomes important as we approach reactor relevant plasma parameters. Since ICRF waves interact with various ion cyclotron resonances and hybrid resonances, there is a variety of phenomena that may occur depending on the ion species and their relative concentrations. The so-called minority heating scheme[1,2], where the launched fast waves are absorbed by a small concentration of seed ion species, is now widely used as a robust and efficient way to heat a plasma.

When a plasma consists of multiple ion species, fast waves encounter two-ion hybrid resonances which exist between the ion cyclotron resonances. At the hybrid resonance, mode conversion from fast waves to ion Bernstein waves (IBWs)[3] or (cold electromagnetic) ion cyclotron waves (ICWs)[4] occurs depending on the plasma parameters and the magnetic field geometry[5,6]. Along the midplane, the fast wave propagation is essentially perpendicular to the magnetic field. At the hybrid resonance, the fast waves convert to pressure driven IBWs which propagate toward the high-field side (Fig. 1(a)). Off the midplane, a finite poloidal magnetic field in the direction of propagation results in an up-shift of the parallel wavenumber. The wave dispersion is altered dramatically and now the the fast waves convert to ICWs which propagate toward the low-field side (Fig. 1 (b)).

The earliest mode conversion heating experiments on tokamaks were performed in D-H plasmas with high-field side antennas[7]. Complete mode conversion to slow waves (IBWs/ICWs) takes place in this scenario, and good heating was observed. Efficient mode conversion heating with the more reactor relevant low-field side antennas were later observed in ^{3}He-H plasmas on TFTR[8], Tore Supra[9,10], ASDEX Upgrade[11] and Alcator C-Mod[12,13], and in D-^{3}He plasmas on Alcator C-Mod[13,14] and JET[15]. It must be noted here that mode conversion to ICWs which can take significant portion of rf power, was neglected in the early analysis of the experimental results. No serious inconsistency was found at the beginning, since direct electron heating, which is a clear sign of mode conversion, occurs around the two-ion hybrid resonance, regardless of whether IBWs or ICWs are excited. ICWs can be absorbed strongly by ions when the minority concentration becomes smaller, but this was somewhat hard to quantify without the aid of two-dimensional full-wave simulations.
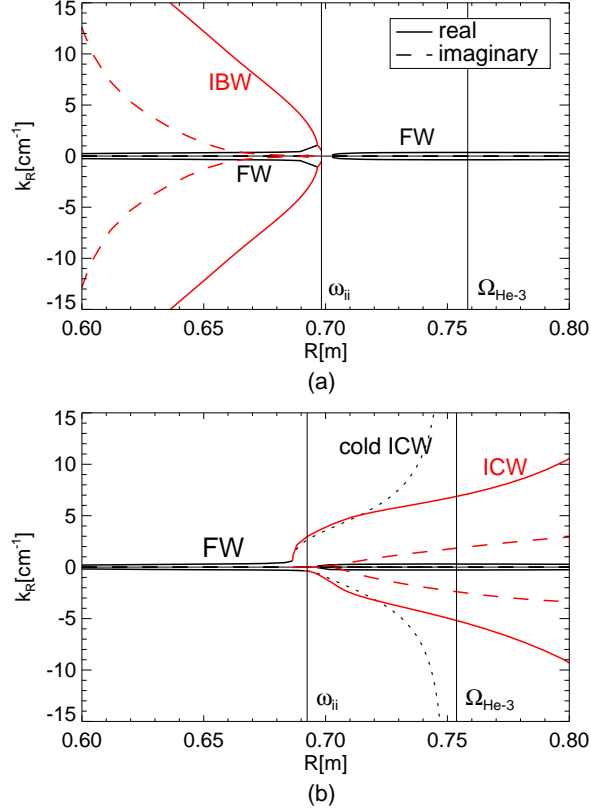
FIG. 1. The local wavenumber in the direction of the major radius on C-Mod (a) along the midplane (b) above the midplane ($Z = 0.12$ m). The cold plasma ICW dispersion is also shown with the dotted curve. The locations of the two-ion hybrid resonance (ω_{ii}) and the helium-3 cyclotron resonance (Ω_{He-3}) are shown with the vertical lines.

When the relevant ion concentrations are comparable and the two-ion hybrid resonance is far away from the cyclotron resonances, mode converted slow waves are absorbed mostly by electrons. Mode conversion current drive[16] has been investigated in the mode conversion electron heating regime on TFTR[8] and Alcator C-Mod[17,18]. Only a small fraction of the total plasma current was driven in these experiments, but in the C-Mod experiment, the sawtooth period could be controlled by placing the hybrid resonance at an appropriate location with respect to the $q = 1$ surface (q is the safety factor). Mode conversion flow drive was observed in D-^{3}He and ^{4}He-^{3}He plasmas on TFTR[19], Alcator C-Mod[20–22] and JET[23]. Optimum flow drive was found at helium-3 concentrations lower than that for efficient mode conversion electron heating, but still high enough for efficient mode conversion ion heating. If sufficient poloidal flow shear can be generated through this method, it may be possible to improve

3

plasma performance by turbulence suppression[24]. Direct rf flow drive has been studied theoretically[25–27], but the full mechanism of flow generation in the presence of rf waves is not well understood, and this is an active area of research.

In order to study the physics of wave interaction with particles that results in current drive or flow drive, a good description of the wave propagation, damping and mode conversion is necessary. Measurements of the waves themselves are particularly important since they serve as a direct test of the relevant wave physics. Scattering of a laser beam has been used on tokamak/stellarator plasmas to measure mode converted IBWs on Microtor[28,29], TFR[30], ACT-1[31], TNT-A[32] and JIPPT-IIU[33], and directly launched IBWs on Alcator C[34]. Some measurements of fast waves were performed with laser scattering[30,35], but the measurements are difficult in general due to the diagnostic limitation at a small wavenumber. Probes were also used to measure IBWs[31] and fast waves[32,35] in some of the above early experiments, when it was possible to insert them into the core of the plasma. The observed wavenumber in these experiments was consistent with the predicted IBW and fast wave dispersion relations. The measured fluctuation amplitude was also analyzed in the TFR experiment, and found to be consistent with theoretical estimates[30].

Phase Contrast Imaging (PCI)[36–38] is capable of measuring rf waves by detecting electron density fluctuations $\tilde{n}_e$, similarly to laser scattering. It is a type of an interferometer, which measures the phase delay $\tilde{\phi}(x)$ introduced by electron density fluctuations that varies over the beam cross section,

$$\tilde{\phi}(x) \simeq -r_e \lambda_0 \int dz \, \tilde{n}_e(x, z), \tag{1}$$

where $r_e = e^2/4\pi\epsilon_0 m_e c^2$ is the classical electron radius, $\lambda_0 (= 10.6 \ \mu\text{m}$ for a CO_2 laser) is the laser wavelength, and z is the distance along the direction of the beam propagation. The advantage of PCI is in its simple response, and the signal is proportional to this phase delay. This allows for a relatively straightforward calibration of the absolute fluctuation intensity (Appendix B). Another advantage is that it is an imaging technique, and the whole spatial fluctuation profile can be obtained simultaneously, whereas for laser scattering, all radial locations and wavenumbers of interest need to be scanned by adjusting the optics. Mode converted ICWs around the Alfvén resonance were observed using PCI on TCA[39,40]. The measured wave intensity was found to be consistent with their numerical simulation. Note that the wave frequency in this experiment was one-tenth of that for typical ICRF heating. The heating power was also small, around 50 kW. The PCI system on Alcator C-Mod

has been used to measure fast waves[41,42], and mode converted waves around the two-ion hybrid resonance[17,21,42–44]. The measured wavenumber and the radial extent of the mode converted wave signal were consistent with full-wave predictions by TORIC[45]. In the C-Mod experiments, the mode converted waves were observed clearly to the low-field side of the two-ion hybrid resonance. Through analysis with TORIC simulations, it was recognized that the observed waves were actually mode converted ICWs, which had been neglected in the analysis prior to this work[43].

Numerical simulations are essential to obtain an accurate description of wave propagation and damping in a plasma which has two-dimensional inhomogeneity. When mode conversion takes place, full-wave treatment is usually necessary. Testing the physics model then becomes a code validation effort, which requires great care in modeling the experiments, especially when the prediction is sensitive to small changes in the input parameters. The TORIC simulation has been compared to PCI measurements on Alcator C-Mod[17,21,42–44], but the comparison was limited to cases where Maxwellian particle distributions could be assumed. In this study, we also used the AORSA[46] code which is coupled to a Fokker-Planck code, CQL3D[47], for self-consistent simulation of wave fields and particle distribution functions[48]. The coupled AORSA-CQL3D simulation gives a fairly complete description of the core rf waves, sufficient for rigorous test of the linear and quasi-linear wave theory in a wide parameter range. Using this simulation, the comparison was extended to minority heating cases. Also, the waves were measured by a carefully calibrated PCI system, and for the first time, extensive comparison of the measured and simulated absolute mode converted wave intensity was performed.

The organization of this paper is as follows. The experimental setup is described in Sec. II. The numerical simulations are briefly described in Sec. III. Measurements and details of the modeling for D-H heating experiments are presented in Sec. IV, and D-^{3}He heating experiments in Sec. V. Results from the two cases are discussed further in Sec. VI, and summarized in Sec. VII.

II. EXPERIMENTAL SETUP

Alcator C-Mod is a compact ($R = 0.67$ m), high field ($B_\phi < 8$ T) tokamak with a diverted geometry[49]. The top view of the tokamak is shown in Fig. 2. Three ICRF antennas are
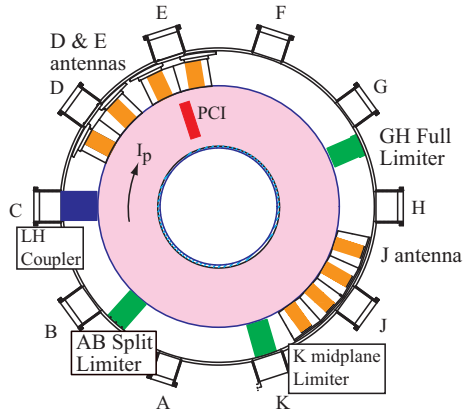
FIG. 2. The top view of the Alcator C-Mod tokamak.

operated at ~80 MHz to heat a plasma through hydrogen minority heating at 5.3 T. The two 2-strap dipole antennas at D and E port are operated at 80.5 and 80.0 MHz, and have 2 MW of source power each[50]. The 4-strap antenna at J port is typically operated at 78 MHz, and has 4 MW of source power[51]. For the results presented in this paper, the straps could be phased as [0, π, π, 0] (180°), [0, $\pi/2$, π, $3\pi/2$] (+90°) and [0, -$\pi/2$, -π, -$3\pi/2$] (-90°). We define positive toroidal angle in the clockwise direction looking down from the top, the same direction as the toroidal magnetic field and the plasma current. The J antenna frequency is tunable between 50-80 MHz. The frequency is changed to 50 MHz to heat D-^{3}He plasmas at the same field (~5 T).

The geometry of the C-Mod PCI system[52] is shown in Fig. 3. A continuous 80 W CO_2 laser (Firestar t60, SYNRAD) is used for measurements. Reflective phase plates were manufactured by Spire, Inc. The complementary area of a ZnSe base was coated with layers of SiO_2, titanium, platinum, and finished with gold such that the groove depth is 1.32 μm ($\pm$ 10%). The beam intensity is imaged with a custom made one dimensional 32-element LN_2 cooled HgCdTe detector array. The detector element size is 750-1000 μm and the distance between the center of the adjacent elements is 850 μm. The bandwidth of the detector together with the preamplifier is ~5 MHz.

Optical heterodyne technique is used to detect ICRF waves at 50-80 MHz. The beam intensity is modulated $I_0(t) = I_0(1 + \cos(\omega_M t))$ so that it beats with the phase perturbation
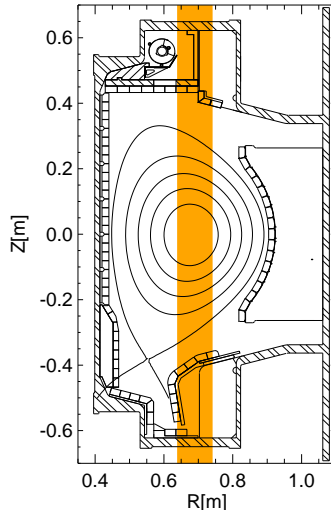
6

FIG. 3. The C-Mod PCI beam geometry.

introduced by the plasma $\tilde{\phi}(t) = \phi \cos(\omega t)$. The beam intensity on the detector $I(t)$ is[38],

$$I(t) = I_0(t)(1 + 2\tilde{\phi}(t)) \tag{2}$$

$$= I_0(1 + \cos(\omega_M t))(1 + 2\phi \cos(\omega t)). \tag{3}$$

Averaging out oscillations at the rf frequencies (ω, ω_M),

$$\overline{I(t)} = I_0(1 + \phi \cos((\omega - \omega_M)t)), \tag{4}$$

and the signal down-shifted to $\omega - \omega_M$ is observed. The modulation is introduced using acousto-optic modulators (N37045, NEOS Technologies, Inc.). The beam is split and sent through the acousto-optic modulators (AOMs) which scatter the laser beam off the sound wave, shifting the laser frequency by the sound wave frequency. When the beams are re-combined, it is modulated at the difference frequency of the split beams.

The efficiency of the AOMs are typically set to 15%, and 6 W is sent into the plasma. The loss in the other optics components up to the detector is about 70%, giving $\sim 1.2 \times 10^2$ W/m^2 for measurements with a 81 mm wide beam. The focusing of the beam on the phase plate is performed using an 80 inch off-axis parabolic mirror. Typically, the phase plate with 1.1 mm groove width is used, which gives the low wavenumber limit $k_R > 1.5$ cm^{-1}. The spatial resolution was $\sim$3 mm, or equivalently, $k_R < 12$ cm^{-1}, for the measurements shown in this paper. The wavenumber of the mode converted slow waves are around $k_R = 3\text{-}10$ cm^{-1}.

7

Note fast waves ($k_R < 1$ cm^{-1}) are filtered out. The PCI diagnostic is located in front of E port (Fig. 2), allowing measurements of the wave field corresponding to 32° (D antenna), 0° (E antenna) and -144° (J antenna) toroidal angles with respect to the three antennas.

To measure electron heating in the mode conversion regime, a second harmonic heterodyne electron cyclotron emission radiometer (FRC-ECE)[53] was used.

III. NUMERICAL SIMULATIONS

Two-dimensional full-wave simulations for an axisymmetric plasma are used to model the ICRF waves. AORSA (All-ORders Spectral Algorithm)[46,54] uses a complete spectral representation of the wave field in Cartesian coordinates, which allows for an immediate evaluation of the susceptibility in the local approximation. The model is valid for arbitrary $k_\perp \rho$ (ρ is the Larmor radius) and cyclotron harmonic number. AORSA is coupled to a Fokker-Planck code, CQL3D (Collisional Quasi-Linear 3D)[47], to simulate self-consistent electric fields and distribution functions[48]. AORSA calculates the quasilinear diffusion coefficients from the electric field solution, which are passed to CQL3D. CQL3D solves the bounce-averaged Fokker-Planck equation in the zero banana width limit, $\rho_{\text{pol}}/a \sim 0$ (ρ_{pol}: poloidal Larmor radius, a: radial scale length). For this work, only the minority ion species was evolved with the rf quasilinear diffusion and collisions with the Maxwellian bulk species. Radial diffusion was turned off. AORSA then solves for the electric field using the plasma dielectric obtained by numerically integrating the distribution function simulated by CQL3D. The process is repeated 4-7 times until the solution converges.

TORIC (TORoidal Ion Cyclotron)[45] solves the reduced finite Larmor radius (FLR) wave equation derived by Swanson[55], Colestock and Kashuba[56] (the SCK model) with relevant electron FLR terms[57]. It should be noted that the reduced FLR dispersion is quantitatively different from the exact one even in the FLR limit in general. Nonetheless, the mode conversion fraction does not depend sensitively on the detail of the slow wave dispersion[5]. Since modification of the wave pattern does not significantly alter the PCI signal, the difference is ignored in the analysis. The dispersion is indeed quantitatively accurate when the majority second harmonic resonance coincides with the minority fundamental resonance, such as in hydrogen minority heating in a deuterium plasma. Since TORIC takes much less computational resource compared to AORSA, it was used extensively in this study.
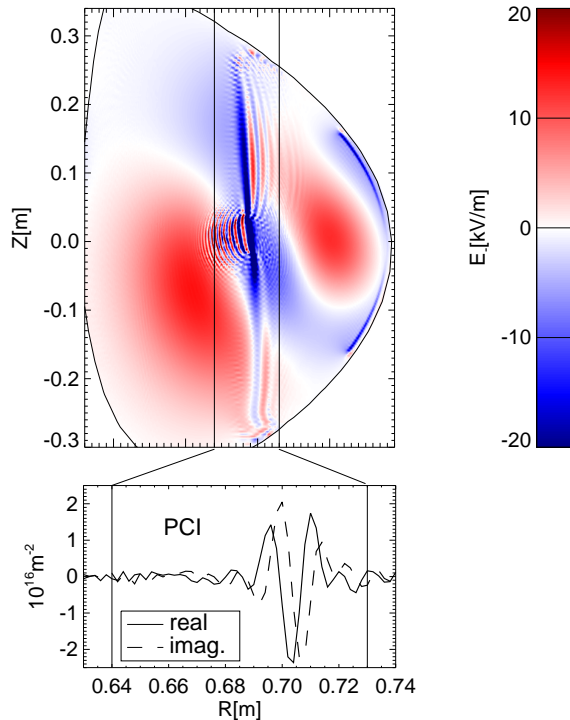
FIG. 4. The left-hand circularly polarized component of the electric field simulated by AORSA (top) and the simulated PCI signal (bottom) in a D-^{3}He plasma, 1 MW rf power.

Comparison of the full-wave simulations and the measurements are performed using a synthetic diagnostic method. The wave electron density fluctuations $\tilde{n}_e$ can be calculated from the electric field solution $\tilde{\mathbf{E}}$ using the modeled electron conductivity operator $\boldsymbol{\sigma}_e$,

$$\tilde{n}_e = \frac{i}{e\omega}\nabla \cdot \tilde{\mathbf{j}}_e = \frac{i}{e\omega}\nabla \cdot (\boldsymbol{\sigma}_e \cdot \tilde{\mathbf{E}}). \tag{5}$$

Due to large parallel electron conductivity, the density fluctuation $\tilde{n}_e$ is dominated by the contribution from $\tilde{E}_\parallel$. The three-dimensional $\tilde{n}_e$ pattern is calculated by summing over solutions of all toroidal mode numbers, integrated along the laser beam path, and the high-pass wavenumber filter of the phase plate and finite resolution of the imaging system (Fig. 22(b)) is applied to "synthesize" the PCI signal. An example of the simulated PCI signal is shown in Fig. 4, together with the corresponding poloidal electric field pattern. The result is compared directly to measurements.
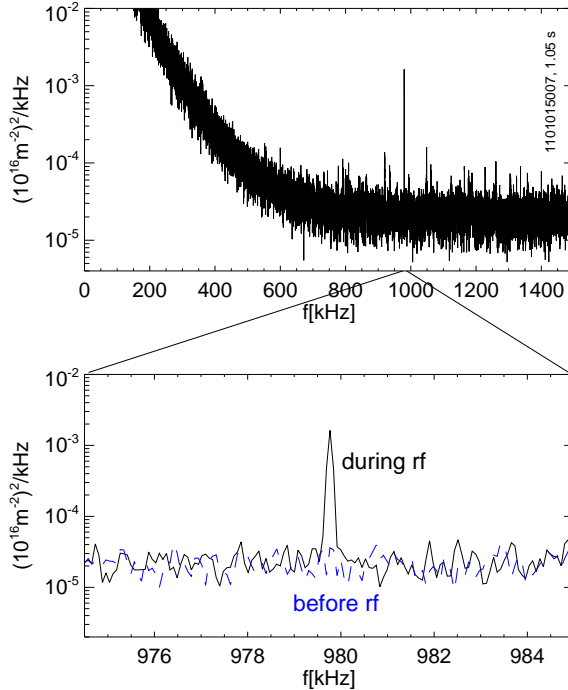
9

FIG. 5. The observed PCI frequency spectrum in a D-H plasma. $n_H/n_e = 0.05$, E antenna, 0.53 MW.

IV. D-H HEATING EXPERIMENT

A typical PCI signal observed in a hydrogen minority heating discharge is shown in Fig. 5. The beam intensity was modulated at 79.02 MHz and a coherent signal ($\delta f < 1$ kHz) can be seen at 0.98 = (80.00 - 79.02) MHz. The broadband fluctuations at $f < 600$ kHz is the plasma turbulence density fluctuations. Although mode conversion is weak in the minority heating regime, the diagnostic is sensitive enough that the mode converted waves can still be observed well. Figure 6 shows the full radial fluctuation intensity profiles and the wavenumber spectra of the mode converted waves observed for two different hydrogen concentrations. The signal is broader at higher minority concentration (b), consistent with weaker damping of the mode converted waves due to large distance between the two-ion hybrid resonance and the hydrogen cyclotron resonance.

Figure 7 shows the comparison of the measured and simulated PCI signals for the discharges shown in Fig. 6. Multiple peaks seen in the radial PCI signal structure are due to line-integration which cancels the net signal at certain radii. The signal depends sensitively
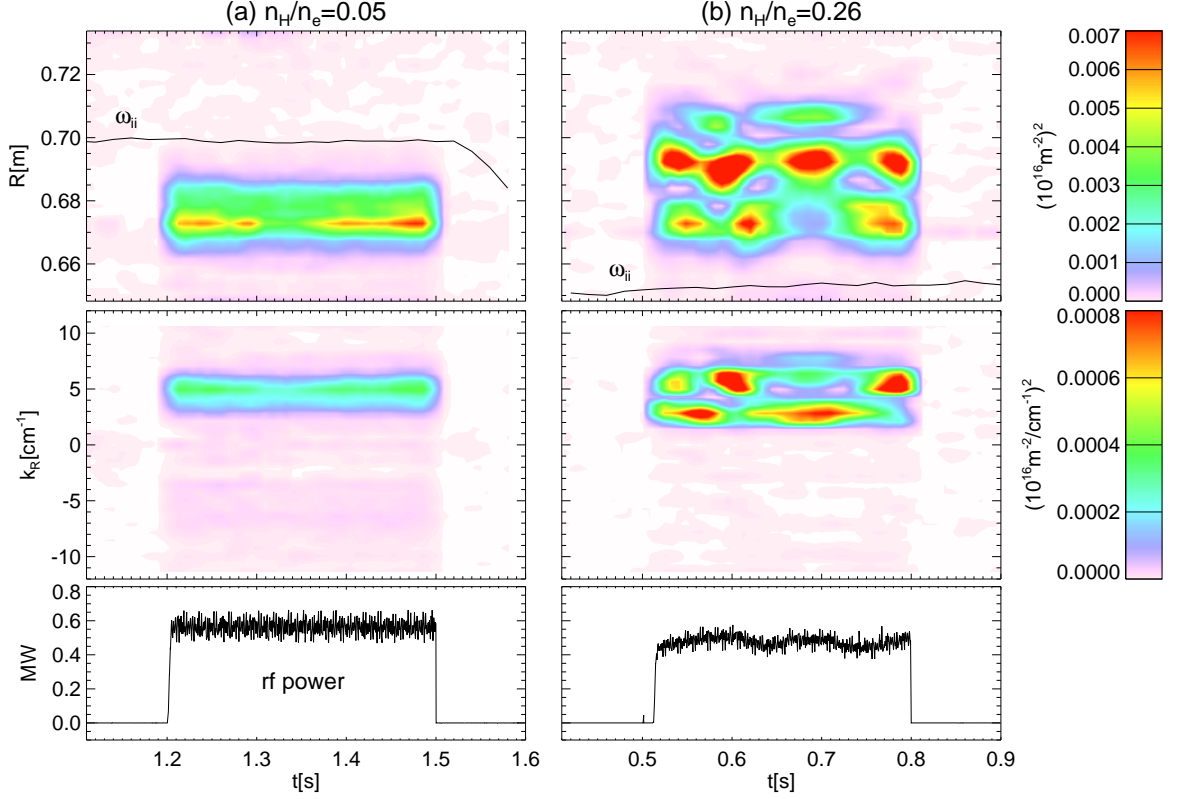
10

FIG. 6. The observed PCI signal with the rf power trace at (a) $n_H/n_e = 0.05$ (b) $n_H/n_e = 0.26$. The locations of the two-ion hybrid resonance layer are also shown with the solid curves (ω_{ii})

on the exact three-dimensional field pattern which is presently not simulated accurately enough to predict these peaks and troughs. Therefore, only the overall fluctuation intensity, signal width and average wavenumber can be compared. The measured and simulated PCI signal widths in D-H plasmas are summarized in Fig. 8. The measured signal width is somewhat narrower than the simulation. There is a possibility of hydrogen concentration estimate error by $\delta(n_H/n_e) \sim -0.06$ at high concentration (Appendix A) which may account for the discrepancy. However, this shift is small enough that it does not alter the picture of the comparison of the wave intensity.

The simulation of the minority heating case shown in Fig. 7(a1,b1) was performed by iterating AORSA and CQL3D. It is important that we do a self-consistent calculation of the electric field and the minority ion distribution function, since the mode converted wave intensity is affected by the deformation of the hydrogen distribution in the minority heating regime. At ~0.5 MW rf power, the measured fluctuation intensity is smaller than what is
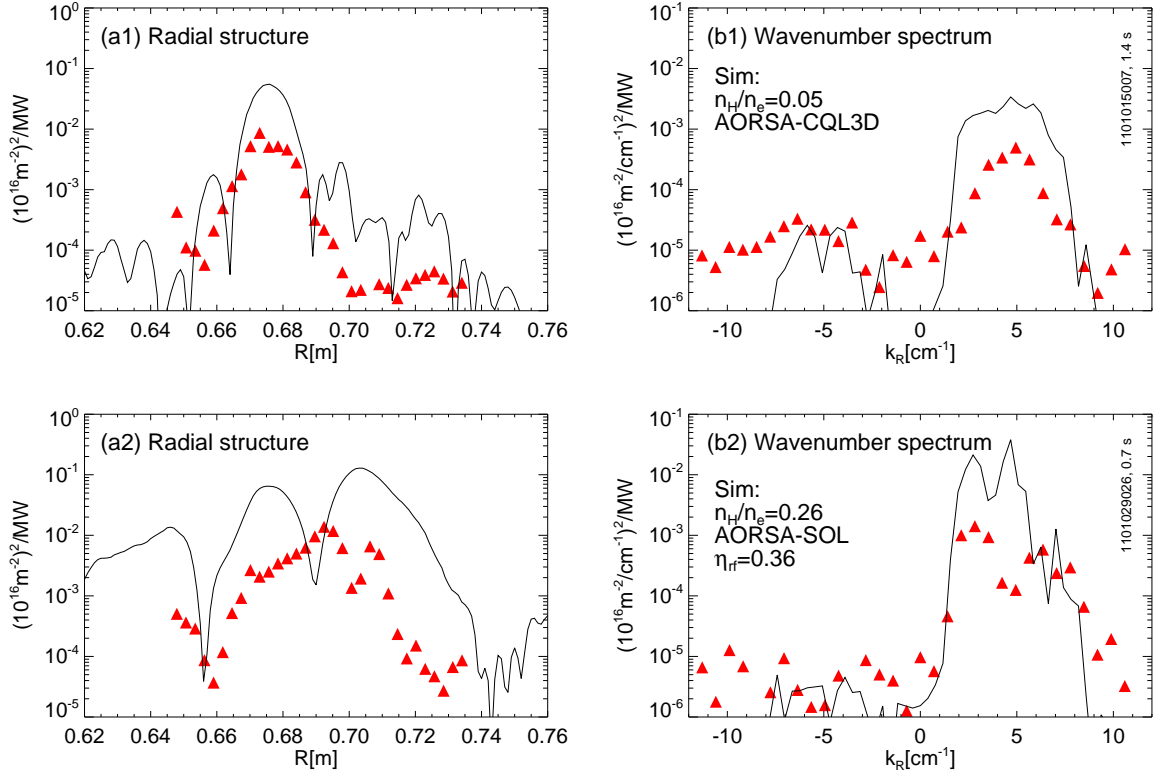
11

FIG. 7. Comparison of the measured and simulated (a*) radial structures (b*) wavenumber spectra of the PCI signals in D-H plasmas. D antenna ($\phi = 32°$). (*1) $n_{\rm H}/n_e = 0.05$, 0.56 MW. Simulation by AORSA-CQL3D. (*2) $n_{\rm H}/n_e = 0.26$, 0.48 MW. Simulation by AORSA-SOL ($\eta_{\rm rf} = 0.36$). Red triangles: measurements. Solid curves: simulations.
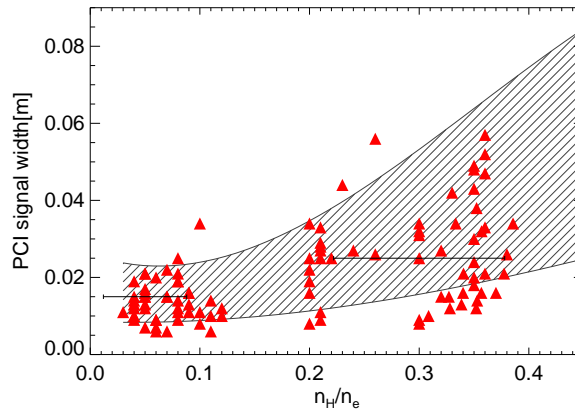

FIG. 8. The measured and simulated PCI signal widths in D-H plasmas. 0.5-1.0 MW rf power. Red triangles: measurements. Hatched area: simulated range of predictions by AORSA-CQL3D at $n_{\rm H}/n_e \leq 0.13$, TORIC and AORSA at $n_{\rm H}/n_e > 0.13$.
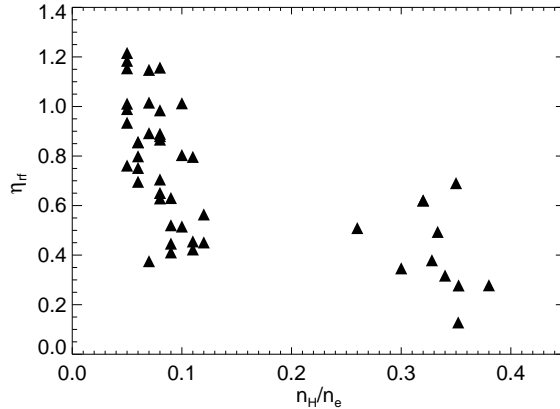
12

FIG. 9. The core absorption efficiency estimated in L-mode D-H plasmas. $\sim$1.0 MW rf power.

predicted by a factor of $\sim$7.

Figure 7(a2,b2) shows the comparison for the high hydrogen concentration case. The modeling of this case is more difficult since both the fast wave minority absorption and the mode conversion fraction are small in this regime. For typical C-Mod parameters, the net single-pass absorption is less than 10%, and the core absorption efficiency needs to be carefully evaluated experimentally. Figure 9 shows the absorption efficiency estimated in L-mode plasmas from change in the magnetic stored energy calculated by EFIT[58]. Because the Ohmic and the rf power density are comparable, change in the confinement time is accounted for by using the L-mode confinement time scaling $\tau_E \sim P^{-1/2}$, which gives,

$$\frac{\eta_{\mathrm{rf}} P_{\mathrm{rf}} + P_{\mathrm{Ohmic},1}}{P_{\mathrm{Ohmic},0}} = \left(\frac{W_{\mathrm{MHD},1}}{W_{\mathrm{MHD},0}}\right)^2. \tag{6}$$

where $W_{\mathrm{MHD},0}$, $W_{\mathrm{MHD},1}$ are the stored energy at the Ohmic and rf phase, $P_{\mathrm{Ohmic},0}$, $P_{\mathrm{Ohmic},1}$ are the Ohmic power at the Ohmic and rf phase, P_{rf} is the launched rf power and η_{rf} is the core absorption efficiency to be estimated. Radiation is small (< 0.1 MW) for these plasmas, and is neglected in the analysis. It can be seen that at $n_{\mathrm{H}}/n_e \sim 0.3$, appreciable amount of power was lost in the edge, and the core absorption efficiency was down to $\eta_{\mathrm{rf}} \sim 0.40$. The simulation domain of AORSA was extended to the scrape-off-layer (SOL) to treat these cases. The results are referred to as AORSA-SOL. Artificial dissipation was introduced to the dielectric in the SOL region to reproduce the reduced core absorption observed in the experiment. Here, the edge dissipation in the code was adjusted so that the core absorption efficiency $\eta_{\mathrm{rf}} = 0.36$. It can be seen that the measured fluctuation intensity is smaller than
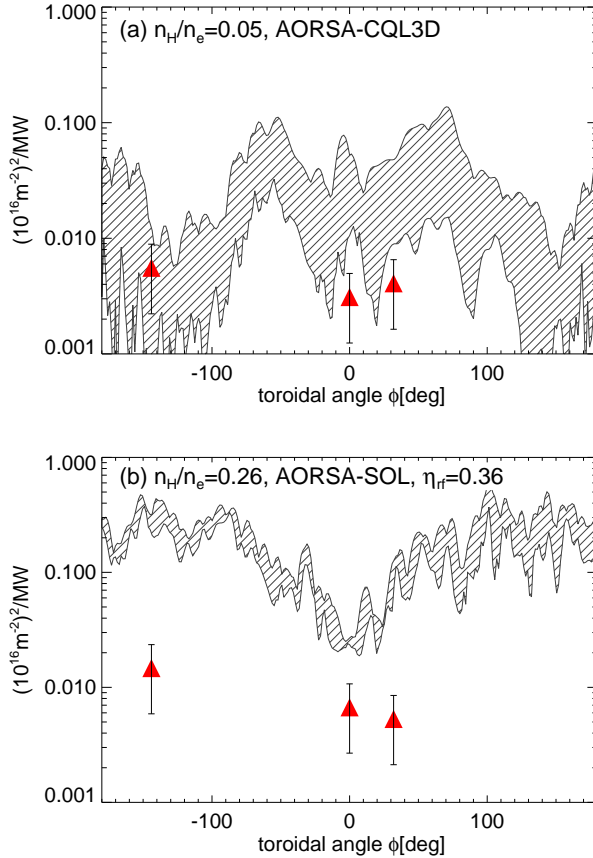
13

FIG. 10. The PCI signal intensity versus the toroidal angle from the antenna. (a) $n_H/n_e \simeq 0.05$, D antenna, 0.56 MW. (b) $n_H/n_e \simeq 0.26$, D antenna, simulation by AORSA-SOL ($\eta_{rf} = 0.36$). Hatched area: simulation. Red triangles: measurements.

the prediction by a factor of ∼13.

Since it is difficult to move the PCI diagnostic and measurements are performed always at the same toroidal location, there is a possibility that the diagnostic is not located at a proper toroidal angle. In order to see if this is the case, the simulated full toroidal variation of the PCI signal for the minority heating case is shown in Fig. 10(a). The uncertainty of the simulation includes the hydrogen concentration error $\delta(n_H/n_e) = \pm 0.01$ and the PCI beam angle error $\delta\theta = \pm 0.06°$. The peaks at $\phi \sim \pm 60°$ are due to second pass of the fast waves, incident to the hybrid resonance from the high-field side. Measured signal intensities from antennas at three different toroidal locations are also shown at the corresponding toroidal angles from the antenna. It can be seen that reasonable signal intensity is expected at all three locations, although they may not be where the predicted signal intensity is maximum.
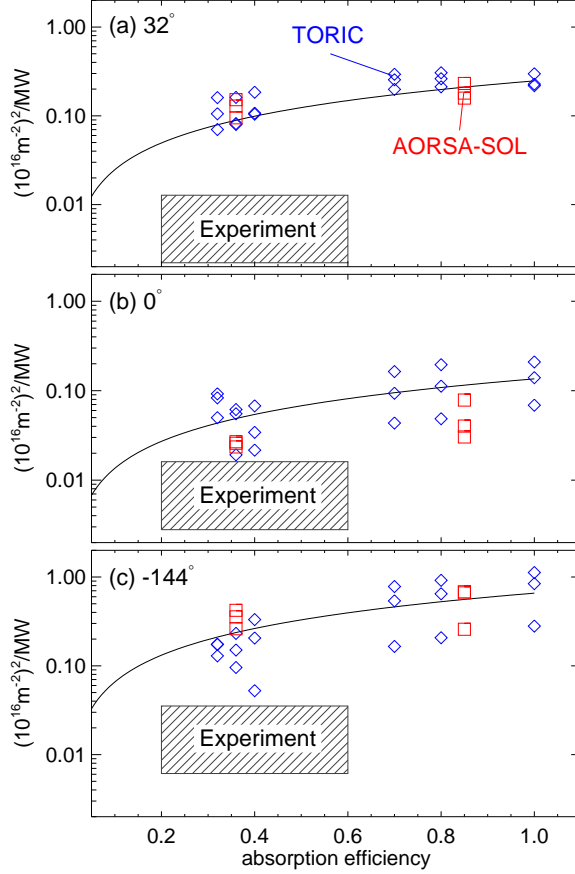
FIG. 11. The simulated PCI signal intensity versus the core absorption at the toroidal angles (a) $\phi = 32°$ (D antenna), (b) $\phi = 0°$ (E antenna), and (c) $\phi = -144°$ (J antenna). $n_{\rm H}/n_e = 0.26$. Blue diamonds: TORIC. Red squares: AORSA-SOL. The curves show ($\eta_{\rm rf}=1.0$ prediction)$\times\eta_{\rm rf}$. The experimentally observed range of the absorption efficiency and the wave intensity is shown with the hatched areas.

The toroidal variation of the signal intensity for the high hydrogen concentration case is shown in Fig. 10(b). The expected signal intensities at the measurement locations are reasonable. In fact, the antenna at -144° is located around the optimum toroidal angle, but the signal intensity is smaller than the simulation by a factor of ~20. The prediction of the high hydrogen concentration cases have additional uncertainty in the estimation of the core absorption efficiency. In order to look at the sensitivity of the prediction to the core absorption efficiency, the simulated signal peak intensity is plotted as a function of the absorption efficiency in Fig. 11. It can be seen that, even taking into account the uncertainty in $\eta_{\rm rf}$, the measured intensity is weaker than predictions by at least a factor of 5. Note that
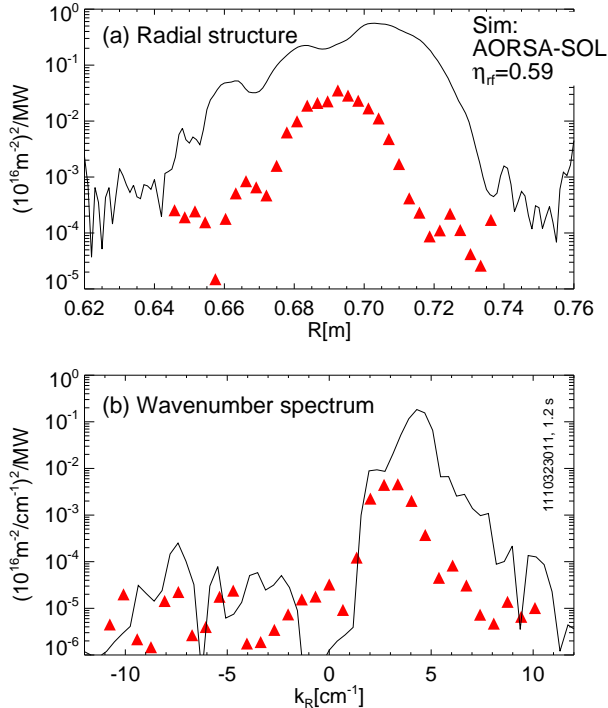
15

FIG. 12. Comparison of the measured and simulated (a) radial structure (b) wavenumber spectrum of the PCI signals in a D-^{3}He plasma. $n_{\text{He-3}}/n_e = 0.22$, J antenna ($\phi = -144°$), 1.4 MW. Red triangles: measurements. Solid curves: simulation by AORSA-SOL ($\eta_{\text{rf}} = 0.59$).

deviation of the full simulation with edge dissipation (symbols) from the value obtained by simply multiplying the absorption efficiency to the perfect absorption result (solid curves) is about a factor of 2. This is not a significant factor for our comparison at this point, but may become important when better accuracy in the wave intensity will be desired.

V.   D-^{3}HE HEATING EXPERIMENT

Comparison of the measured PCI signal and the simulation by AORSA in a D-^{3}He plasma is shown in Figure 12. Similarly to D-H plasmas, the exact signal structure cannot be reliably compared. Summary of the comparison of the measured and simulated PCI signal widths in D-^{3}He plasmas is shown in Fig. 13. The measured signal width may be somewhat narrower than what is predicted.

Mode conversion is expected to be strong in D-^{3}He plasmas, and indeed, the measured signal intensity in Fig. 12 is appreciably stronger than that in D-H plasmas (cf. Fig. 7).
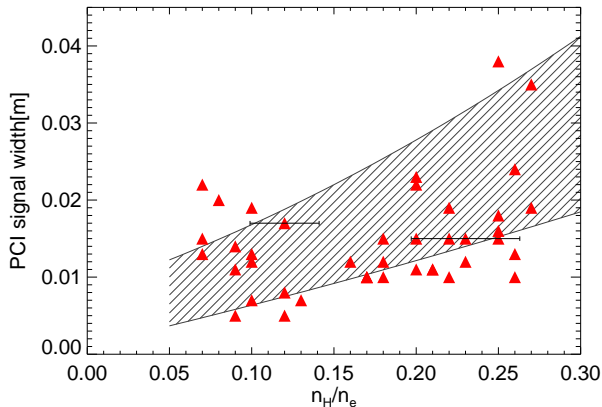
16

FIG. 13. The measured and the simulated PCI signal width in D-^{3}He plasmas. 0.5 MW rf power. Red triangles: measurements. Hatched area: simulation by AORSA-CQL3D at $n_{\text{He-3}}/n_e \leq 0.13$, TORIC and AORSA at $n_{\text{He-3}}/n_e > 0.13$.
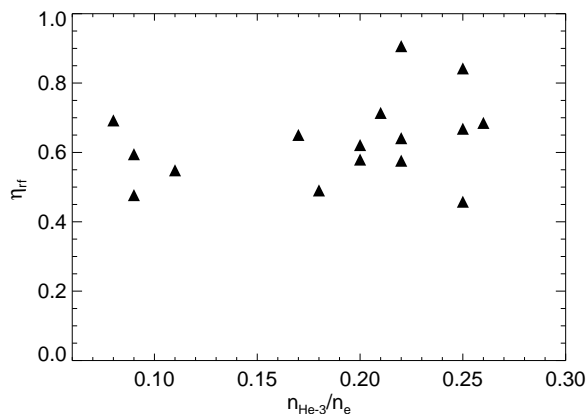

FIG. 14. The absorption efficiency estimated in L-mode D-^{3}He plasmas. $\sim$1.0 MW rf power.

However, the measured absolute signal intensity is only a few percent of the simulated value in this case.

Single-pass absorption is $\sim$30% for these plasmas, and finite power loss is often observed. Figure 14 shows the core absorption efficiency estimated from change in the magnetic stored energy. It can be seen that typically, $\eta_{\text{rf}} \sim 0.7$, and it is also relatively insensitive to the helium-3 concentration. Mode conversion in D-^{3}He plasmas is accompanied by strong direct electron heating. The electron heating power density was obtained from ECE break-in-slope analysis[59,60] and compared to simulations in Fig. 15. The difference between the TORIC and AORSA profiles is because of the difference in the mode converted slow wave pattern
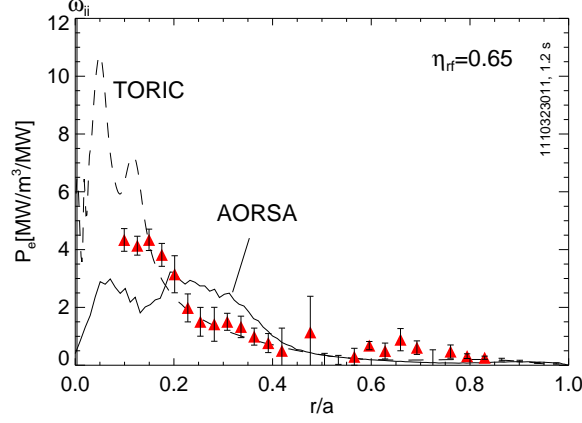
17

FIG. 15. The measured and simulated ($\eta_{\text{rf}} = 0.65$) rf electron heating power density. Red triangles: measurements. Solid curve: AORSA. Dashed curve: TORIC.
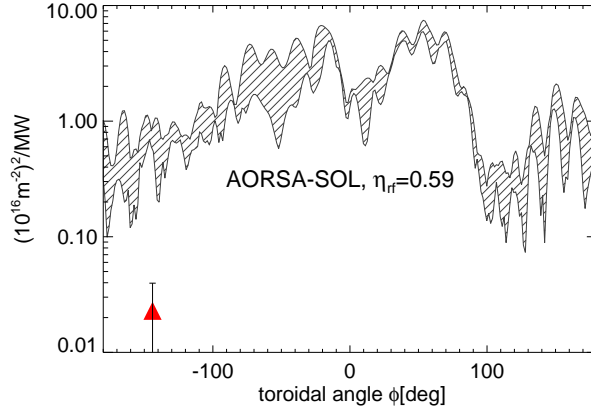

FIG. 16. The PCI signal intensity versus the toroidal angle from the antenna, at $n_{\text{He-3}}/n_e \simeq 0.22$, $\eta_{\text{rf}} = 0.59$. Hatched area: simulation by AORSA-SOL. Red triangles: measurements.

due to the usage of the reduced-FLR dielectric in TORIC. The measured heating power density agrees with the simulation with $\eta_{\text{rf}} = 0.65$, consistent with the estimate from the stored energy change.

The toroidal variation of the simulated signal is shown in Fig. 16. The measurement is a factor of $\sim$30 smaller than the prediction. Measurements at high helium-3 concentration could be performed only using J antenna which could be operated at 50 MHz. It can be seen that the fluctuation intensity is small in the region where the measurements were performed. However, looking at the measurements in D-H plasmas using three antennas (Fig. 10), it appears unlikely that uncertainty in the simulated toroidal variation would result in this
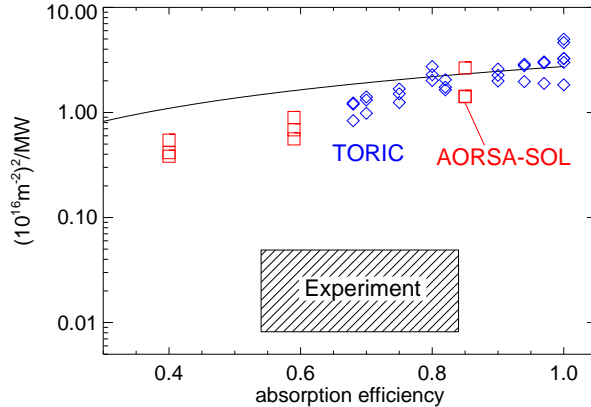
18

FIG. 17. The simulated PCI signal intensity versus the core absorption at $\phi = -144°$ (J antenna). $n_{\text{He-3}}/n_e = 0.22$. Blue diamonds: TORIC. Red squares: AORSA-SOL. The curve shows (η_{rf}=1.0 prediction)$\times\eta_{\text{rf}}$. The experimentally observed range of the absorption efficiency and the wave intensity is shown with the hatched area.

large discrepancy.

The simulated signal intensity is shown as a function of the absorption efficiency in Fig. 17. The simulated wave intensity is at least a factor of $\sim$20 stronger than the measurements. Typically, the discrepancy is closer to a factor of $\sim$50. Note that simply multiplying the perfect absorption result with the absorption efficiency (solid curve) instead of introducing the edge power loss (symbols) gives a prediction that is larger by a factor of $\sim$2.

VI. WAVE INTENSITY DEPENDENCE

The measured and simulated mode converted wave intensities in D-H and D-^{3}He plasmas as seen by PCI are summarized in Fig. 18. The detail of the modeling for D-H and D-^{3}He plasmas are described in Sec. IV and V, respectively. It is clear from the plot that the measured mode converted wave intensity is substantially weaker than what is predicted when the wave intensity is stronger: 100%-14% of the prediction in the D-H minority heating regime (blue squares); 8% of the prediction in the high hydrogen concentration regime (green downward-triangles); 2% of the prediction in the D-^{3}He mode conversion regime (red upward-triangles). This is not explicable by uncertainty in the measured core absorption efficiency, since the uncertainty is the largest in the high hydrogen concentration regime despite the
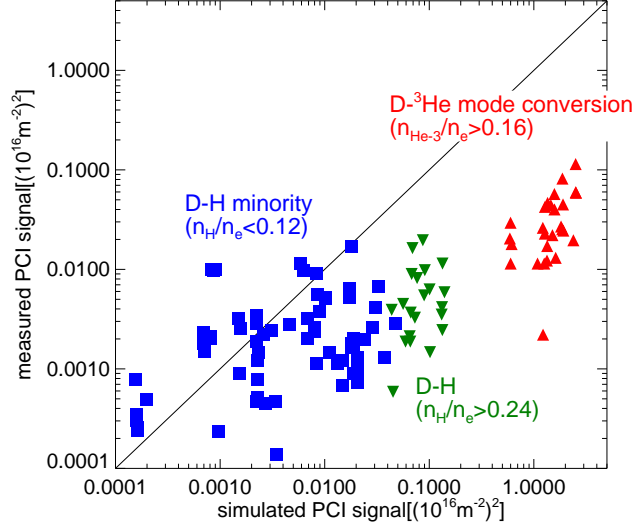
19

FIG. 18. The measured versus the simulated PCI signal intensity. Simulation by AORSA.

fact that this is not where we see the largest discrepancy. Agreement is poor in the D-^{3}He mode conversion regime, even though the measured core absorption efficiency is reasonable ($\eta_{\mathrm{rf}} \sim 0.65$, see Fig. 14).

From the electron heating results in Sec. V or previous experiments[14,15], fast waves certainly undergo a process that results in strong electron heating with the efficiency consistent with the linear mode conversion theory. This is in apparent contradiction with our wave intensity measurements here. However, noting the "universality" of the Budden tunneling factor[5], the efficiency of electron heating may be relatively insensitive to the exact detail of the mode conversion process as long as some dissipation is present.

We know from past experiments that linear theory describes electrostatic waves only in the small amplitude limit and that theory breaks down easily due to processes such as trapping in the large wave amplitude, parametric decay instabilities, etc. Nonlinear damping on half ion cyclotron harmonics is experimentally observed in the context of ICRF mode conversion[61], although this exact process does not apply here since we observe strong electron heating. Parametric decay instabilities (PDI)[62,63] may reduce the pump wave intensity without significantly affecting the electron heating. In the electron cyclotron frequency regime, PDI was observed around the upper hybrid resonance[64]. Upper hybrid soliton can also form around the resonance[65,66], which may have implications for the mode conversion physics. Therefore, it is not obvious that the linear theory should be valid for all our results,

and larger deviation from the linear theory at higher wave intensity observed here may be an indication of nonlinear wave physics being involved in the pertinent mode conversion process.

VII. CONCLUSIONS AND FUTURE WORK

Mode converted waves were measured over a range of ion species concentrations in D-H and D-^{3}He plasmas using a phase contrast imaging diagnostic on Alcator C-Mod. The measurements were compared to predictions of the full-wave simulation codes AORSA and TORIC. AORSA was iterated with the CQL3D Fokker-Planck solver, to simulate self-consistent electric fields and a minority ion distribution function. The measured wavenumber and the radial extent of the mode converted wave were consistent with the full-wave predictions. Comprehensive study of the mode converted wave intensity was performed for the first time, and the trends of the measured and simulated intensities were found to be consistent. The absolute intensity of the measurements and simulations also agreed when the wave intensity was weak. However, the measured intensity was a factor of $\sim$50 weaker than predicted in the D-^{3}He mode conversion regime where the wave intensity was strong.

In order to improve the modeling in the weak absorption regimes, the core absorption efficiency was estimated from the change in the stored energy and artificial edge dissipation was introduced in the simulations to account for this edge power loss. This was important for modeling high hydrogen concentration cases and D-^{3}He mode conversion cases where single-pass absorption was not very high. Although the uncertainty in the estimated core absorption was large, the simulated overall wave field was not very sensitive to this error and the wave field intensity could be predicted with reasonable accuracy in the presence of edge loss. Simulations were performed with a scrape-off-layer plasma using AORSA, but this did not reduce the discrepancy. Although realistic edge modeling is missing in TORIC and AORSA, this result suggests that the core rf field is fairly insensitive to details of the edge modeling. That being said, sensitivity to the antenna modeling was not investigated extensively, and some improvement may still be possible with an accurate edge and antenna modeling.

The ion species concentration profiles were assumed to be flat in all the simulations. There is slight difference in the concentration estimated from the observation of mode con-

version which reflects the core, and spectroscopy measurements looking at the divertor region (Fig. 20, Fig. 4 in Ref.[15]). However, the peaking in the concentration that can be inferred from the difference is too small to alter the prediction significantly. Charge exchange recombination spectroscopy to measure the hydrogen and helium distribution function is being installed on Alcator C-Mod, which will be useful to investigate this point further.

The simulations for the hydrogen minority heating cases are sensitive to the non-thermal minority distribution function. Since zero banana width was assumed in the CQL3D simulations performed in this paper, possible finite orbit effects are neglected. However, the same AORSA-CQL3D simulation has been compared to minority distribution function measurements using a neutral particle analyzer[67]. Although there still remain some issues with the time dependent simulation, the simulated steady state distribution function appears to be in reasonable agreement with the measurements, and it is not very likely that the predicted mode conversion efficiency would be in serious error in the framework of quasi-linear theory.

Considering the large discrepancy that we observe at high wave intensity, it is not likely that improvements in the above mentioned aspects of the model will fully resolve the discrepancy. These results call for investigation of the possible importance of nonlinear phenomena in the context of mode conversion, for which little work has been done to date.

ACKNOWLEDGMENTS

Appendix A: Estimation of the Minority Ion Species Concentration

The location of the two-ion hybrid resonance layer is determined primarily by the ion species concentrations. The dependence can be used to give a rough estimate of the core
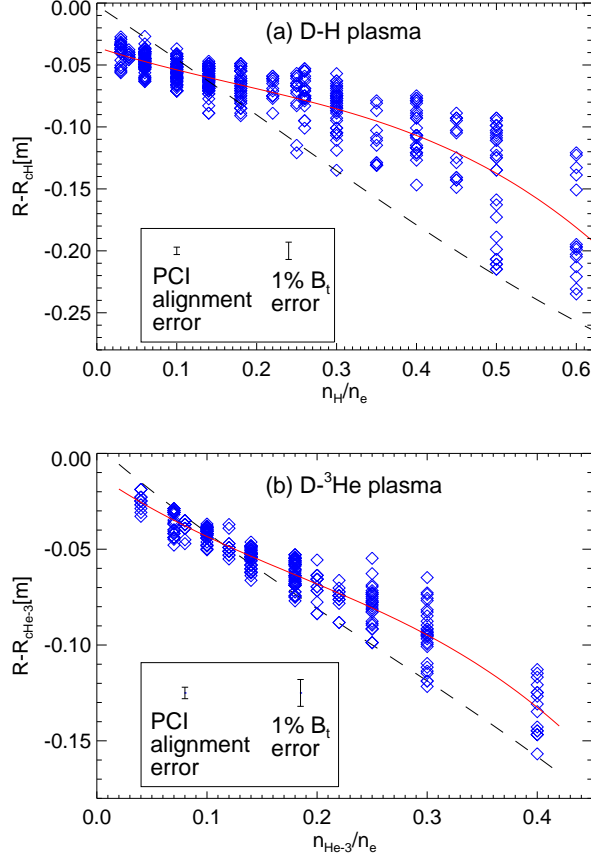
FIG. 19. The simulated PCI signal peak location with respect to the minority ion cyclotron resonance in (a) D-H plasmas (b) D-^{3}He plasmas. The red solid curve is the fit through the simulation points. The two-ion hybrid resonance location is shown with the solid dashed curve (ω_{ii}).

minority ion concentration from the radial location of the PCI signal. The simulated major radius of the PCI signal peak with respect to the hydrogen cyclotron resonance is shown in Fig. 19(a). Multiple peak radii for a given concentration are due to random change in the radial structure of the signal for slightly different plasma profiles and PCI beam angles ($\delta\theta = 0.06°$). The hybrid resonance layer location and the fitted curve can be used to quickly estimate the hydrogen concentration from the radial profile of the observed PCI signal. The alignment error or the toroidal field error may lead to a systematic error of $\delta(n_{\mathrm{H}}/n_e) \sim 0.04$. Due to large uncertainty in the peak location, estimated concentration of any given single discharge may be off by ~ 0.1 especially at high concentration. However, since this is a random scatter, the overall trend can be obtained reasonably well by improving statistics by
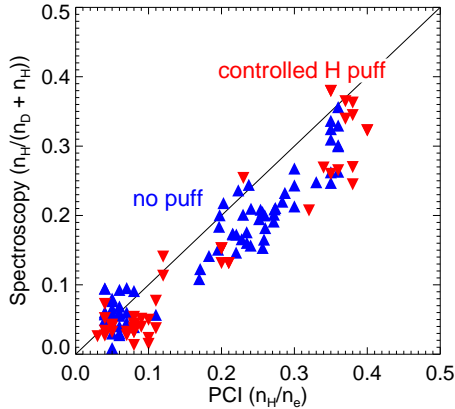
23

FIG. 20. The hydrogen concentration estimated from PCI and spectroscopy. Blue upward-triangles: plasmas with no extra hydrogen puff, naturally occuring; Red downward-triangles: plasmas with controlled hydrogen puff.

collecting results obtained at different antenna frequencies or from discharges with slightly different plasma parameters. The same kind of plot used to estimate helium-3 concentration in D-^{3}He plasmas is shown in Fig. 19(b).

Figure 20 compares the concentration estimated with PCI and the H_α/D_α spectroscopy measurement looking at the divertor region[68] in plasmas with and without external hydrogen puff. It can be seen that the PCI estimates are consistently higher than the spectroscopy measurements. If the concentration estimated by PCI is off by $\delta(n_H/n_e) \sim -0.06$ at $n_H/n_e = $ 0.2-0.3, this would correspond to 0.01 m offset of the hybrid resonance location seen by PCI. If this were all due to the toroidal field error, the value reported by EFIT would be higher than reality by 1-2%, which is larger than the toroidal field measurement calibration error <1%. It should be noted that since PCI reflects the core n_H/n_e whereas spectroscopy measures n_H/n_D in the divertor region, it is not necessary that these two estimates agree. All the concentration estimates in this paper are from PCI since it is available regardless of the magnetic geometry. Using estimates from the H_α/D_α spectroscopy measurement instead does not alter the conclusion presented in this paper.
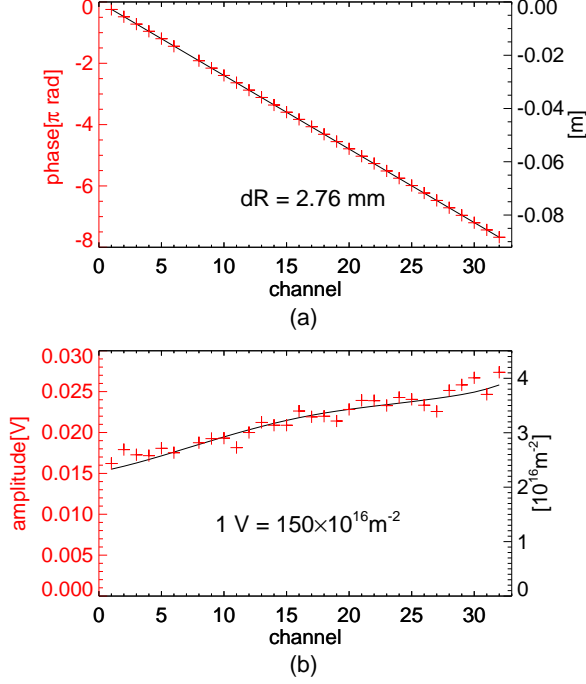
24

FIG. 21. The measured (a) phase (b) voltage amplitude of the sound wave.

Appendix B: Calibration of the PCI Diagnostic

Sound waves produced by a calibrated ultrasound speaker is measured ∼0.3 s before the plasma discharge to calibrate the diagnostic. The calibration of the sources themselves was done using a calibrated microphone (model 377A50, PCB Piezotronics, Inc., calibration by West Caldwell Calibration Laboratories, Inc., traceable to NIST). The measured sound wave profiles were fit to a model function, and integrated to give the line-integrated pressure fluctuation. The result is converted to the CO_2 laser phase delay and to the corresponding line-integrated electron density of a plasma.

The measured sound wave signal at 15 kHz, 2.7 cm^{-1} is shown in Fig. 21. The phase change from channel to channel (a) is used to determine the spacing of the detector elements mapped to the object plane, or equivalently, the magnification of the imaging optics. Since the optical axis is aligned accurately, only the magnification is needed to map each detector elements to the tokamak major radius. The measured detector spacing is 2.76 mm in this case, 10% off from the nominal value 3.14 mm. The measured voltage amplitude (b) is used to obtain the absolute fluctuation amplitude calibration. The solid curve shows the equivalent electron density fluctuation from the loudspeaker calibration. The response is
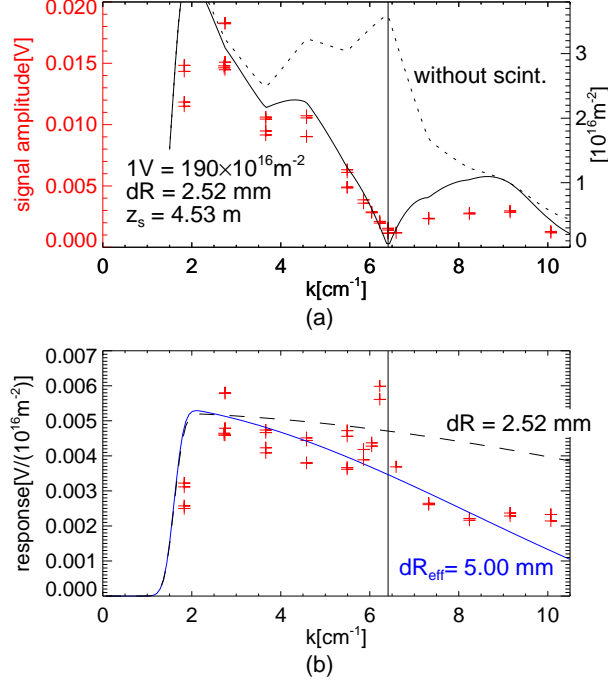
FIG. 22. (a) The measured signal amplitude versus the wavenumber (red plus symbols). The source calibration curve with and without scintillation is shown with the solid and the dotted curves. (b) The response of the system versus the wavenumber (red plus symbols). Black dashed curve: the ideal response. Blue solid curve: the response for an effective resolution of 5.0 mm.

typically around ~ 1 V/$(150 \times 10^{16}$m$^{-2})$.

The wavenumber response is not entirely flat and also needs to be tested. The loudspeaker frequency is scanned to measure the wavenumber response of the system. The result is shown in Fig. 22. The calibration sources are placed outside of the machine, 5.03 m away from the tokamak midplane where the object plane of the imaging optics is located. The null of the response in Fig. 22(a) (the solid curve or the measurement points) infers 4.53 m distance from the object plane. This means that the actual object plane is 0.5 m below the tokamak midplane, which also corresponds to 10% error from the nominal distance. This offset is not corrected, but it affects the signal intensity by at most a few percent and negligible. Figure 22(b) shows the wavenumber response of the system, which is lower than the expected curve (black dashed curve). There seem to be some aberration problems, which results in the effective resolution of the system of ~ 5.00 mm (blue solid curve).

REFERENCES

[1] T. H. Stix, "Fast-wave heating of a two-component plasma," Nuclear Fusion, **15**, 737 (1975).

[2] M. Porkolab, "Plasma heating by fast magnetosonic waves in Tokamaks," AIP Conference Proceedings, **314**, 99 (1994), advances in Plasma Physics Thomas H. Stix Symposium.

[3] I. B. Bernstein, "Waves in a Plasma in a Magnetic Field," Phys. Rev., **109**, 10 (1958).

[4] T. Stix, *Waves in Plasmas* (American Institute of Physics, New York, 1992) p. 32.

[5] D. G. Swanson, "Radio frequency heating in the ion-cyclotron range of frequencies," Physics of Fluids, **28**, 2645 (1985).

[6] F. Perkins, "Heating tokamaks via the ion-cyclotron and ion-ion hybrid resonances," Nuclear Fusion, **17**, 1197 (1977).

[7] J. Adam, "Review of Tokamak plasma heating by wave damping in the ion cyclotron range of frequency," Plasma Physics and Controlled Fusion, **29**, 443 (1987).

[8] R. Majeski, J. H. Rogers, S. H. Batha, R. Budny, E. Fredrickson, B. Grek, K. Hill, J. C. Hosea, B. LeBlanc, F. Levinton, M. Murakami, C. K. Phillips, A. T. Ramsey, G. Schilling, G. Taylor, J. R. Wilson, and M. C. Zarnstorff, "Mode Conversion Heating and Current Drive Experiments in TFTR," Phys. Rev. Lett., **76**, 764 (1996).

[9] B. Saoutic, A. Bécoulet, T. Hutter, D. Fraboulet, A. K. Ram, and A. Bers, "Mode Conversion Heating Experiments on the Tore Supra Tokamak," Phys. Rev. Lett., **76**, 1647 (1996).

[10] I. Monakhov, Y. Petrov, V. Basiuk, A. Becoulet, and F. Nguyen, "Power deposition profiles during FW-IBW mode conversion on Tore Supra: Measurements and simulations," AIP Conference Proceedings, **485**, 136 (1999).

[11] J.-M. Noterdaeme, M. Brambilla, B. Br'usehaber, R. Dux, H.-U. Fahrbach, W. Becker, F. Braun, H. Faugel, D. Hartmann, F. Hofmeister, F. Wesner, and A. U. Team, "He3 in H, Ion Cyclotron Resonance Frequency Mode Conversion and Minority Heating Experiments in ASDEX Upgrade," in *26th EPS Conf. on Contr. Fusion and Plasma Physics, Maastricht, 14 - 18 June 1999* (1999).

[12] Y. Takase, R. L. Boivin, F. Bombarda, P. T. Bonoli, C. L. Fiore, D. Garnier, J. A. Goetz, S. N. Golovato, R. S. Granetz, M. J. Greenwald, S. F. Horne, A. E. Hubbard, I. H. Hutchinson, J. H. Irby, H. Kimura, R. Majeski, E. S. Marmar, M. May, A. Mazurenko,

P. O'Shea, R. Pinsker, M. Porkolab, J. Reardon, J. E. Rice, C. Rost, J. Schachter, J. A. Snipes, P. Stek, J. L. Terry, R. L. Watterson, B. Welch, and S. M. Wolfe, "Survey of ICRF heating experiments and enhanced performance modes in Alcator C-Mod," Plasma Physics and Controlled Fusion, **38**, 2215 (1996).

[13]P. T. Bonoli, P. O'Shea, M. Brambilla, S. N. Golovato, A. E. Hubbard, M. Porkolab, Y. Takase, R. L. Boivin, F. Bombarda, C. Christensen, C. L. Fiore, D. Garnier, J. Goetz, R. Granetz, M. Greenwald, S. F. Horne, I. H. Hutchinson, J. Irby, D. Jablonski, B. LaBombard, B. Lipschultz, E. Marmar, M. May, A. Mazurenko, G. McCracken, R. Nachtrieb, A. Niemczewski, H. Ohkawa, D. A. Pappas, J. Reardon, J. Rice, C. Rost, J. Schachter, J. A. Snipes, P. Stek, K. Takase, J. Terry, Y. Wang, R. L. Watterson, B. Welch, and S. M. Wolfe, "Electron heating via mode converted ion Bernstein waves in the Alcator C-Mod tokamak," Physics of Plasmas, **4**, 1774 (1997).

[14]P. T. Bonoli, M. Brambilla, E. Nelson-Melby, C. K. Phillips, M. Porkolab, G. Schilling, G. Taylor, S. J. Wukitch, R. L. Boivin, C. J. Boswell, C. L. Fiore, S. Gangadhara, J. Goetz, R. Granetz, M. Greenwald, A. E. Hubbard, I. H. Hutchinson, Y. In, J. Irby, B. LaBombard, B. Lipschultz, E. Marmar, A. Mazurenko, R. Nachtrieb, D. Pappas, C. S. Pitcher, J. Reardon, J. Rice, W. L. Rowan, J. A. Snipes, Y. Takase, J. Terry, and S. M. Wolfe, "Mode conversion electron heating in Alcator C-Mod: Theory and experiment," Physics of Plasmas, **7**, 1886 (2000).

[15]M. Mantsinen, M.-L. Mayoral, D. V. Eester, B. Alper, R. Barnsley, P. Beaumont, J. Bucalossi, I. Coffey, S. Conroy, M. de Baar, P. de Vries, K. Erents, A. Figueiredo, A. Gondhalekar, C. Gowers, T. Hellsten, E. Joffrin, V. Kiptily, P. Lamalle, K. Lawson, A. Lyssoivan, J. Mailloux, P. Mantica, F. Meo, F. Milani, I. Monakhov, A. Murari, F. Nguyen, J.-M. Noterdaeme, J. Ongena, Y. Petrov, E. Rachlew, V. Riccardo, E. Righi, F. Rimini, M. Stamp, A. Tuccillo, K.-D. Zastrow, M. Zerbini, and J. E. contributors, "Localized bulk electron heating with ICRF mode conversion in the JET tokamak," Nuclear Fusion, **44**, 33 (2004).

[16]R. Majeski, C. K. Phillips, and J. R. Wilson, "Electron Heating and Current Drive by Mode Converted Slow Waves," Phys. Rev. Lett., **73**, 2204 (1994).

[17]S. J. Wukitch, Y. Lin, A. Parisot, J. C. Wright, P. T. Bonoli, M. Porkolab, N. Basse, E. Edlund, A. Hubbard, L. Lin, A. Lynn, E. Marmar, D. Mossessian, P. Phillips, and G. Schilling, "Ion cyclotron range of frequency mode conversion physics in Alcator C-Mod:

Experimental measurements and modeling," Physics of Plasmas, **12**, 056104 (2005).

[18]A. Parisot, S. J. Wukitch, P. Bonoli, M. Greenwald, A. Hubbard, Y. Lin, R. Parker, M. Porkolab, A. K. Ram, and J. C. Wright, "Sawtooth period changes with mode conversion current drive on Alcator C-Mod," Plasma Physics and Controlled Fusion, **49**, 219 (2007).

[19]C. Phillips, M. Bell, R. Bell, S. Bernabei, M. Bettenhausen, C. Bush, D. Clark, D. Darrow, E. Fredrickson, G. Hanson, J. Hosea, B. LeBlanc, R. Majeski, S. Medley, R. Nazikian, M. Ono, H. Park, M. Petrov, J. Rogers, G. Schilling, C. Skinner, D. Smithe, E. Synakowski, G. Taylor, and J. Wilson, "ICRF heating and profile control techniques in TFTR," Nuclear Fusion, **40**, 461 (2000).

[20]Y. Lin, J. E. Rice, S. J. Wukitch, M. J. Greenwald, A. E. Hubbard, A. Ince-Cushman, L. Lin, M. Porkolab, M. L. Reinke, and N. Tsujii, "Observation of Ion-Cyclotron-Frequency Mode-Conversion Flow Drive in Tokamak Plasmas," Phys. Rev. Lett., **101**, 235002 (2008).

[21]Y. Lin, J. E. Rice, S. J. Wukitch, M. J. Greenwald, A. E. Hubbard, A. Ince-Cushman, L. Lin, E. S. Marmar, M. Porkolab, M. L. Reinke, N. Tsujii, and J. C. W. and, "Observation of ion cyclotron range of frequencies mode conversion plasma flow drive on Alcator C-Mod," Physics of Plasmas, **16**, 056102 (2009), ISSN 1070664X.

[22]Y. Lin, J. Rice, S. Wukitch, M. Reinke, M. Greenwald, A. Hubbard, E. Marmar, Y. Podpaly, M. Porkolab, N. Tsujii, and the Alcator C-Mod team, "ICRF mode conversion flow drive on Alcator C-Mod," Nuclear Fusion, **51**, 063002 (2011).

[23]Y. Lin, P. Mantica, T. Hellsten, E. Lerche, M. Nave, J. Rice, D. V. Eester, P. C. de Vries, R. Felton, C. Giroud, V. Kiptily, T. Tala, and J. E. contributors, "ICRF mode conversion flow drive in JET D(^{3}He) plasmas and comparison with results from Alcator C-Mod," in *37th EPS Conf. on Plasma Physics and Controlled Fusion, Dublin, Ireland, June 2010*, P5.164 (2010).

[24]E. F. Jaeger, L. A. Berry, and D. B. Batchelor, "Full-wave calculation of sheared poloidal flow driven by high-harmonic ion Bernstein waves in tokamak plasmas," Physics of Plasmas, **7**, 3319 (2000).

[25]J. R. Myra and D. A. D'Ippolito, "Toroidal formulation of nonlinear-rf-driven flows," Physics of Plasmas, **9**, 3867 (2002).

[26]E. F. Jaeger, L. A. Berry, J. R. Myra, D. B. Batchelor, E. D'Azevedo, P. T. Bonoli, C. K.

Phillips, D. N. Smithe, D. A. D'Ippolito, M. D. Carter, R. J. Dumont, J. C. Wright, and R. W. Harvey, "Sheared Poloidal Flow Driven by Mode Conversion in Tokamak Plasmas," Phys. Rev. Lett., **90**, 195001 (2003).

[27] J. R. Myra, L. A. Berry, D. A. D'Ippolito, and E. F. Jaeger, "Nonlinear fluxes and forces from radio-frequency waves with application to driven flows in tokamaks," Physics of Plasmas, **11**, 1786 (2004).

[28] P. Lee, R. J. Taylor, W. A. Peebles, H. Park, C. X. Yu, Y. Xu, N. C. Luhmann, and S. X. Jin, "Observation of Mode-Converted Ion Bernstein Waves in the Microtor Tokamak," Phys. Rev. Lett., **49**, 205 (1982).

[29] H. Park, N. C. Luhmann, W. A. Peebles, and R. Kirkwood, "Observation of Second-Harmonic Ion Bernstein Waves Excited by Fast-Wave Mode Conversion in the Microtor Tokamak," Phys. Rev. Lett., **52**, 1609 (1984).

[30] TFR Group, A. Truc, and D. Gresillon, "Observation of fast and slow modes associated with ICRF heating in the TFR tokamak by CO_2 laser scattering," Nuclear Fusion, **22**, 1577 (1982).

[31] G. A. Wurden, M. Ono, and K. L. Wong, "Ion-temperature measurement via laser scattering on ion Bernstein waves," Phys. Rev. A, **26**, 2297 (1982).

[32] K. Ida, O. Naito, I. Ochiai, S. Shinohara, and K. Miyamoto, "Observation of fast wave and mode-converted ion Bernstein wave by magnetic probes and 2-mm microwave scattering," Nuclear Fusion, **24**, 375 (1984).

[33] T. Tetsuka, K. Kawahata, S. Okajima, A. Nishizawa, T. Watari, R. Ando, S. Tanahashi, K. Toi, and J. Fujita, "Observation of Mode-Converted Ion Bernstein Wave by an HCN Laser Scattering," Journal of the Physical Society of Japan, **54**, 3757 (1985).

[34] Y. Takase, J. D. Moody, C. L. Fiore, F. S. McDermott, M. Porkolab, and J. Squire, "Study of directly launched ion Bernstein waves in a tokamak," Phys. Rev. Lett., **59**, 1201 (1987).

[35] H. Park, W. A. Peebles, N. C. L. Jr, R. Kirkwood, and R. J. Taylor, "Observation of the externally excited fast magnetosonic wave via collective Thomson scattering," Plasma Physics and Controlled Fusion, **27**, 1195 (1985).

[36] F. Zernike, "Das phasenkontrastverfahren bei der mikroskopischen beobachtung," Zeitschrift für technische Physik, **16**, 454 (1935).

[37] F. Zernike, "How I Discovered Phase Contrast," Science, New Series, **121**, 345 (1955),

ISSN 00368075.

[38]H. Weisen, "The phase contrast method as an imaging diagnostic for plasma density fluctuations (invited)," Review of Scientific Instruments, **59**, 1544 (1988).

[39]H. Weisen, G. Borg, B. Joye, A. J. Knight, and J. B. Lister, "Measurements of the Tokamak-Safety-Factor Profile by Means of Driven Resonant Alfvén Waves," Phys. Rev. Lett., **62**, 434 (1989).

[40]H. Weisen, K. Appert, G. G. Borg, B. Joye, A. J. Knight, J. B. Lister, and J. Vaclavik, "Mode conversion to the kinetic Alfvén wave in low-frequency heating experiments in the TCA tokamak," Phys. Rev. Lett., **63**, 2476 (1989).

[41]E. Nelson-Melby, A. Mazurenko, M. Porkolab, P. T. Bonoli, and S. J. Wukitch, "Phase contrast imaging of ion Bernstein and fast waves in Alcator C-Mod," AIP Conference Proceedings, **595**, 90 (2001), rADIO FREQUENCY POWER IN PLASMAS:14th Topical Conference.

[42]E. Nelson-Melby, *Observations and Theory of Mode-Converted Ion Bernstein Waves in the Alcator C-Mod Tokamak*, Ph.D. thesis, Massachusetts Institute of Technology, Cambridge, MA 02139 (2002).

[43]E. Nelson-Melby, M. Porkolab, P. T. Bonoli, Y. Lin, A. Mazurenko, and S. J. Wukitch, "Experimental Observations of Mode-Converted Ion Cyclotron Waves in a Tokamak Plasma by Phase Contrast Imaging," Phys. Rev. Lett., **90**, 155004 (2003).

[44]Y. Lin, S. Wukitch, A. Parisot, J. C. Wright, N. Basse, P. Bonoli, E. Edlund, L. Lin, M. Porkolab, G. Schilling, and P. Phillips, "Observation and modelling of ion cyclotron range of frequencies waves in the mode conversion region of Alcator C-Mod," Plasma Physics and Controlled Fusion, **47**, 1207 (2005).

[45]M. Brambilla, "Numerical simulation of ion cyclotron waves in tokamak plasmas," Plasma Physics and Controlled Fusion, **41**, 1 (1999).

[46]E. F. Jaeger, L. A. Berry, E. D'Azevedo, D. B. Batchelor, and M. D. Carter, "All-orders spectral calculation of radio-frequency heating in two-dimensional toroidal plasmas," Physics of Plasmas, **8**, 1573 (2001).

[47]R. W. Harvey and M. G. McCoy, "CQL3D Fokker-Planck code," in *Proceedings of the IAEA Technical Committee Meeting on Simulation and Modeling of Thermonuclear Plasmas, Montreal, Canada, 1992 (USDOC NTIS Document No. DE93002962)* (1992) p. 40, eDB/700350;.

[48]E. Jaeger, R. Harvey, L. Berry, J. Myra, R. Dumont, C. Phillips, D. Smithe, R. Barrett, D. Batchelor, P. Bonoli, M. Carter, E. D'azevedo, D. D'ippolito, R. Moore, and J. Wright, "Global-wave solutions with self-consistent velocity distributions in ion cyclotron heated plasmas," Nuclear Fusion, **46**, S397 (2006).

[49]I. H. Hutchinson, R. Boivin, F. Bombarda, P. Bonoli, S. Fairfax, C. Fiore, J. Goetz, S. Golovato, R. Granetz, M. Greenwald, S. Horne, A. Hubbard, J. Irby, B. LaBombard, B. Lipschultz, E. Marmar, G. McCracken, M. Porkolab, J. Rice, J. Snipes, Y. Takase, J. Terry, S. Wolfe, C. Christensen, D. Garnier, M. Graf, T. Hsu, T. Luke, M. May, A. Niemczewski, G. Tinios, J. Schachter, and J. Urbahn, "First results from Alcator-C-MOD," Physics of Plasmas, **1**, 1511 (1994).

[50]Y. Takase, S. Golovato, M. Porkolab, K. Bajwa, H. Becker, and D. Caldwell, "Engineering design and analysis of the Alcator C-MOD two-strap ICRF antenna," in *Fusion Engineering, 1991. Proceedings., 14th IEEE/NPSS Symposium on* (1991) pp. 118–121 vol.1.

[51]S. J. Wukitch, R. L. Boivin, P. T. Bonoli, J. A. Goetz, J. Irby, I. Hutchinson, Y. Lin, A. Parisot, M. Porkolab, E. Marmar, G. Schilling, and J. R. Wilson, "Investigation of performance limiting phenomena in a variable phase ICRF antenna in Alcator C-Mod," Plasma Physics and Controlled Fusion, **46**, 1479 (2004).

[52]M. Porkolab, J. Rost, N. Basse, J. Dorris, E. Edlund, L. Lin, Y. Lin, and S. Wukitch, "Phase contrast imaging of waves and instabilities in high temperature magnetized fusion plasmas," IEEE Transactions on Plasma Science, **34**, 229 (2006), ISSN 0093-3813, 32nd International Conference on Plasma Science (ICOPS 2005), Monterey, CA, JUN, 2005.

[53]J. W. Heard, C. Watts, R. F. Gandy, P. E. Phillips, G. Cima, R. Chatterjee, A. Blair, A. Hubbard, C. W. Domier, and N. C. Luhmann, "High resolution electron cyclotron emission temperature profile and fluctuation diagnostic for Alcator C-Mod," Review of Scientific Instruments, **70**, 1011 (1999), ISSN 00346748.

[54]E. F. Jaeger, L. A. Berry, E. D'Azevedo, D. B. Batchelor, M. D. Carter, K. F. White, and H. Weitzner, "Advances in full-wave modeling of radio frequency heated, multidimensional plasmas," Physics of Plasmas, **9**, 1873 (2002).

[55]D. G. Swanson, "Derivation of the mode conversion-tunneling equation from the Vlasov equation," Physics of Fluids, **24**, 2035 (1981).

[56]P. Colestock and R. Kashuba, "The theory of mode conversion and wave damping near the ion cyclotron frequency," Nuclear Fusion, **23**, 763 (1983).

[57] M. Brambilla, "Finite Larmor radius wave equations in Tokamak plasmas in the ion cyclotron frequency range," Plasma Physics and Controlled Fusion, **31**, 723 (1989).

[58] L. Lao, H. S. John, R. Stambaugh, A. Kellman, and W. Pfeiffer, "Reconstruction of current profile parameters and plasma shapes in tokamaks," Nuclear Fusion, **25**, 1611 (1985).

[59] D. Gambier, M. Evrard, J. Adam, A. Becoulet, S. Corti, P. Hennequin, J. Jacquinot, D. Start, K. Thomsen, B. Tubbing, and V. Zanza, "ICRF power deposition profile and determination of the electron thermal diffusivity by modulation experiments in JET," Nuclear Fusion, **30**, 23 (1990).

[60] E. A. Lerche, D. V. Eester, and J. E. contributors, "Improved break-in-slope analysis of the plasma energy response in tokamaks," Plasma Physics and Controlled Fusion, **50**, 035003 (2008).

[61] F. Nguyen, J.-M. Noterdaeme, I. Monakhov, F. Meo, H. Fahrbach, C. Maggi, R. Neu, W. Suttrop, M. Brambilla, D. Hartmann, F. Wesner, and A. U. Team, "ICRF Ion Heating with Mode Conversion on the Tokamak ASDEX Upgrade," in *29th EPS Conf. on Plasma Physics and Controlled Fusion, Montreux, Switzerland, June 2002*, P1.045 (2002).

[62] R. V. Nieuwenhove, G. V. Oost, J.-M. Noterdaeme, M. Brambilla, J. Gernhardt, and M. Porkolab, "Parametric decay in the edge plasma of ASDEX during fast wave heating in the ion cyclotron frequency range," Nuclear Fusion, **28**, 1603 (1988).

[63] M. Porkolab, "Invited paper: Parametric instabilities in the tokamak edge plasma in the ion cyclotron heating regimes," Fusion Engineering and Design, **12**, 93 (1990), ISSN 0920-3796.

[64] F. S. McDermott, G. Bekefi, K. E. Hackett, J. S. Levine, and M. Porkolab, "Observation of the parametric decay instability during electron cyclotron resonance heating on the Versator II tokamak," Physics of Fluids, **25**, 1488 (1982).

[65] M. Porkolab and M. V. Goldman, "Upper-hybrid solitons and oscillating-two-stream instabilities," Physics of Fluids, **19**, 872 (1976).

[66] T. Cho and S. Tanaka, "Observation of an Upper-Hybrid Soliton," Phys. Rev. Lett., **45**, 1403 (1980).

[67] A. C. Bader, *Experimental Measurements and Numerical Modeling of Fast-ion Distributions in the Alcator C-Mod Tokamak*, Ph.D. thesis, Massachusetts Institute of Technology, Cambridge, MA 02139 (2012).

[68]T. E. Tutt, *H-α/D-α Spectroscopy on Alcator C-Mod*, Master's thesis, Massachusetts Institute of Technology, Cambridge, MA 02139 (1999).